

NONLINEAR RADIATION EFFECT  
ON CASSON FLUID SATURATED NON-DARCY POROUS MEDIUM

N. VIJAYA, K. SREELAKSHMI\* AND G. SAROJAMMA

Department of Applied Mathematics,  
Sri Padmavati Mahila Visvavidyalayam, Tirupati - 517502, India.

(Received On: 12-01-17; Revised & Accepted On: 01-02-17)

---

ABSTRACT

*This paper deals with the study of MHD non-Darcy Casson fluid flow induced due to a vertical porous stretching surface in the presence of nonlinear thermal radiation, viscous dissipation and first order chemical reaction. Similarity variables have been employed to transform the governing non-linear boundary layer equations into a set of non-linear ordinary differential equations. Numerical solutions are obtained for the velocity, temperature and concentration using shooting technique and Runge - Kutta method. Comparison of our results under limiting cases is made with the already published results. To understand the influence of the physical parameters, flow characteristics are evaluated and graphically presented for different variations of governing parameters. The Nusselt number and Sherwood number are also evaluated and discussed.*

**Keywords:** Casson fluid, non-linear thermal radiation, non-Darcy porous medium, viscous dissipation.

---

1. INTRODUCTION

Study of non-Newtonian fluids is gaining importance due to its diverse range of applications in industry. Some examples of such fluids are lubricants, colloidal and suspension solutions, polymer solutions, fruit juice, paints etc. In non-Newtonian fluids, the relation between shear stress and shear rate is non-linear and hence, apparent viscosity of the fluid is not a constant. Various constitutive equations have been developed to describe a non-Newtonian fluid suitably. Casson fluid is one non-Newtonian fluid proposed by Casson to describe the flow curves of suspension of pigments in Lithographic varnishes used for printing inks. It is reported that this model described accurately the flow curves of suspensions of bentonite in water [1], suspension of Silicon [2] and several polymers [3] used in industry. Blood is also modeled as a Casson fluid as blood shows a Newtonian nature when it flows through larger diameter vessels and shows a highly non-Newtonian behavior while flowing through the smaller diameter vessels. Literature reveals that studies on heat and mass transfer in Casson fluid flows are very limited. Some of the researchers focused their study on these aspects in Casson fluids under different conditions [4–9].

Fluid flows over stretching surfaces have several industrial applications including extrusion of polymer or rubber sheets, glass blowing and continuous casting. In melt-spinning process, the extrudate from the die is drawn and stretched into a filament or sheet and is solidified by gradual cooling with water or chilled metal rolls. Heat transfer at the sheet has an important role on the quality of the final product. Extensive research has been done on stretching flows under different configurations.

Heat transfer in porous media plays a crucial role in different applications such as extraction of crude oil, thermal insulation and chemical reactors. Significant work has been reported on heat transfer in Darcy porous medium. Darcy law is valid when the flow rate is small. At higher rates of flow there is a variation from Darcy nature and non-Darcy nature prevails. The Darcy- Forchheimer model describes the effect of inertia as well as viscous forces in porous media. A detail review on heat transfer in Darcian and non-Darcian porous medium is found in Nield and Bejan [10].

Heat transfer in fluid flows over a stretching sheet due to thermal radiation has significant industrial applications in solar power technology, furnace design, solar ponds, heat exchangers, satellites and space vehicles. Recently, the concept of non-linear thermal radiative heat transfer has been introduced [11–13]. The presence of non-linear thermal radiation makes the energy equation strongly non-linear.

---

**Corresponding Author: K. Sreelakshmi\*, Department of Applied Mathematics,  
Sri Padmavati Mahila Visvavidyalayam, Tirupati - 517502, India.**

The objective of this analysis is to investigate the effect of non-linear thermal radiation and viscous heating on the MHD non-Darcy flow of an incompressible and electrically conducting Casson fluid induced due to a stretching surface.

## 2. MATHEMATICAL FORMULATION

Consider the steady non-Darcy mixed convective heat and mass transfer of an incompressible and electrically conducting Casson fluid flow induced by a vertical stretching sheet embedded in a fluid saturated porous medium. A Cartesian coordinate system is taken with x-axis along the sheet and y-axis normal to the sheet as shown in Fig. 1. The flow region is subjected to a uniform transverse magnetic field  $\vec{B} = (0, B_0, 0)$  and uniform electric field  $\vec{E} = (0, 0, -E_0)$ . It is assumed that the flow is generated by stretching of an elastic boundary sheet by imposing two equal and opposite forces in such a way that velocity of the boundary sheet is of linear order of the flow direction. The Maxwell's equations are  $\nabla \cdot \vec{B} = 0$  and  $\nabla \times \vec{E} = 0$ . From the Ohm's law  $\vec{J} = \sigma(\vec{E} + \vec{q} \times \vec{B})$ , where  $\vec{J}$  is the Joule current,  $\sigma$  is the magnetic permeability and  $\vec{q}$  is the fluid velocity. The induced magnetic field due to the motion of the electrically conducting fluid is negligible. Temperature and species concentration are assumed to have quadratic variations with the distance from origin.

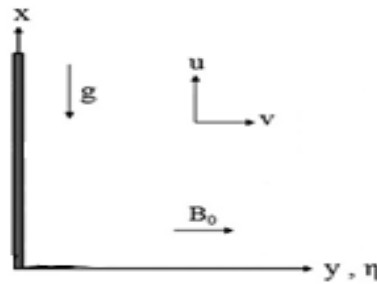


**Fig. 1:** Physical model and coordinate system

Constitutive equation of the Casson fluid can be written as

$$\tau_{ij} = \begin{cases} 2\left(\mu_B + \frac{P_y}{\sqrt{2\pi}}\right) e_{ij}, & \pi > \pi_c \\ 2\left(\mu_B + \frac{P_y}{\sqrt{2\pi_c}}\right) e_{ij}, & \pi < \pi_c \end{cases} \quad (1)$$

where  $\tau_{ij}$  is the  $(i, j)^{\text{th}}$  component of the stress tensor,  $\mu_B$  is the plastic dynamic viscosity of the non-Newtonian fluid,  $P_y$  is the yield stress of the fluid,  $\pi$  is the product of the component of deformation rate with itself, namely,  $\pi = e_{ij} e_{ij}$ , and  $e_{ij}$  is the  $(i, j)^{\text{th}}$  component of deformation rate, and  $\pi_c$  is the critical value of  $\pi$  based on the non-Newtonian model.

By applying boundary layer approximations, the governing equations are expressed as follows:

$$\frac{\partial u}{\partial x} + \frac{\partial v}{\partial y} = 0, \quad (2)$$

$$\frac{1}{\varepsilon} \left( u \frac{\partial u}{\partial x} + v \frac{\partial u}{\partial y} \right) = \frac{\nu}{\varepsilon} \left( 1 + \frac{1}{\beta} \right) \frac{\partial^2 u}{\partial y^2} + \frac{\sigma}{\rho} (E_0 B_0 - B_0^2 u) - \frac{\nu}{k_1} u - \frac{C_b}{\sqrt{k_1}} u^2, \quad (3)$$

$$u \frac{\partial T}{\partial x} + v \frac{\partial T}{\partial y} = \frac{k}{\rho C_p} \frac{\partial^2 T}{\partial y^2} + \frac{16\sigma^*}{3k^* \rho C_p} \frac{\partial}{\partial y} \left( T^3 \frac{\partial T}{\partial y} \right) + \frac{\mu}{\rho C_p} \left( 1 + \frac{1}{\beta} \right) \left( \frac{\partial u}{\partial y} \right)^2 \quad (4)$$

$$u \frac{\partial C}{\partial x} + v \frac{\partial C}{\partial y} = D \frac{\partial^2 C}{\partial y^2} - k_0 (C - C_\infty), \quad (5)$$

where  $u$  and  $v$  are the fluid velocity components along  $x$  and  $y$  axes, respectively,  $\varepsilon$  is the porosity of the medium,  $\nu$  is the kinematic viscosity,  $\rho$  is the density of the fluid,  $E_0$  is the electric field strength in the transverse direction,  $B_0$  is the transverse magnetic field strength,  $k_1$  is the permeability of porous medium,  $\beta = \mu_B \sqrt{2\pi_c} / P_y$  is the Casson parameter,  $C_b$  is the form of drag coefficient which is independent of viscosity and other physical properties of the fluid which depend on the geometry of the medium,  $T$  is the temperature of the fluid inside the thermal boundary layer,  $T_w$  is the uniform temperature and  $T_\infty$  is the fluid temperature in the free stream with  $T_w > T_\infty$ ,  $C$  is the fluid concentration,  $C_w$  is the uniform concentration and  $C_\infty$  is the fluid concentration in the free stream with  $C_w > C_\infty$ ,  $c_p$  is the specific heat at constant pressure,  $\mu$  is the dynamic viscosity of the fluid,  $k$  is the thermal conductivity of the medium,  $\sigma^*$  is the Stefan-Boltzman constant and  $k^*$  is the absorption coefficient,  $D$  is the mass diffusivity and  $k_0$  is the chemical reaction. Boundary conditions are:

$$\begin{aligned} u &= u_w(x) + N \left( 1 + \frac{1}{\beta} \right) \nu \frac{\partial u}{\partial y}, \quad v = v_w, \quad T = T_w = T_\infty + A_0 \left( \frac{x}{l} \right)^2, \quad C = C_w = C_\infty + A_1 \left( \frac{x}{l} \right)^2 \quad \text{at } y = 0, \\ u &\rightarrow 0, \quad T \rightarrow T_\infty, \quad C \rightarrow C_\infty \quad \text{as } y \rightarrow \infty, \end{aligned} \quad (6)$$

where  $u_w(x) = bx$  is the velocity of the stretching surface,  $b$  is the proportionality constant of the stretching velocity,  $A_0$  and  $A_1$  are the parameters of temperature and concentration distributions respectively on the stretching surface, is the parameter of distribution on the stretching surface.

To solve the governing boundary layer equations (3) – (5), the following similarity transformations are introduced:

$$u = bx f'(\eta), v = -\sqrt{bv} f(\eta), \eta = \sqrt{\frac{b}{v}} y, \quad \theta(\eta) = \frac{T-T_\infty}{T_w-T_\infty}, \quad \phi(\eta) = \frac{C-C_\infty}{C_w-C_\infty} \quad (7)$$

Substitution of equation (7) into the governing equations (3) – (5) and using the above relations we finally obtain a system of non-linear ordinary differential equations

$$\left(1 + \frac{1}{\beta}\right) \frac{f'''}{\varepsilon} + \frac{f f''}{\varepsilon^2} - \frac{f'^2}{\varepsilon^2} + M^2(E_I - f') - F^* f'^2 - k_p f' = 0, \quad (8)$$

$$\theta'' + Nr[(1 + (\theta_w - 1)\theta)^3] \theta'' + 3Nr[(\theta_w - 1)(1 + (\theta_w - 1)\theta)^2] \theta'^2 + Pr[f\theta' - 2f'\theta + Ec\left(1 + \frac{1}{\beta}\right)(f'')^2] = 0, \quad (9)$$

$$\phi'' + Sc(f\phi' - 2f'\phi - \gamma\phi) = 0, \quad (10)$$

Boundary conditions (6) reduce to:

$$f(0) = 0, f'(0) = 1, \theta(0) = 1, \phi(0) = 1 \text{ at } \eta = 0, \quad (11)$$

$$f'(\infty) = 0, \theta(\infty) = 0, \phi(\infty) = 0 \text{ as } \eta \rightarrow \infty, \quad (12)$$

where primes denote differentiation with respect to  $\eta$ ,  $M^2 = \sigma B_0^2 / \rho b$  is magnetic parameter,  $k_p = \nu / k_1 b$  is porous parameter,  $E_I = E_0 / B_0 b x$  is electric field parameter,  $F^* = \frac{C_b x}{\sqrt{k_1}}$  is inertial parameter,  $Pr = \rho c_p \nu / k$  is Prandtl number,  $Nr = 16 \sigma^* T_\infty^3 / 3 k k^*$  is thermal radiation parameter,  $\theta_w = T_w / T_\infty$  is temperature ratio parameter,  $Ec = b^2 l^2 / c_p A_0$  is Eckert number,  $Sc = \nu / D$  is Schmidt number,  $\gamma = k_0 / b$  is chemical reaction parameter.

The Physical quantities of engineering interest in this problem are the skin friction coefficient  $C_f$ , Nusselt number  $Nu_x$  and Sherwood number  $Sh_x$ . The skin friction coefficient  $C_f$ , is defined by

$$C_f = \frac{2\tau_w}{\rho u_w^2}, \quad (13)$$

where the wall shear stress  $\tau_w$  is given by

$$\tau_w = \mu \left( \frac{\partial u}{\partial y} \right)_{y=0}. \quad (14)$$

Using the non-dimensional variables equation (7), we get from equations (13) and (14) as

$$\frac{1}{2} C_f \sqrt{Re_x} = \left(1 + \frac{1}{\beta}\right) f''(0). \quad (15)$$

The local Nusselt number which is defined as

$$Nu_x = \frac{x q_w}{K(T_w - T_\infty)}, \quad (16)$$

where  $q_w$  is the heat transfer from the sheet is given by

$$q_w = -K \left( \frac{\partial T}{\partial y} \right)_{y=0}. \quad (17)$$

Using the non-dimensional variables (7), we get from equations (16) and (17) as

$$Nu_x / Re_x^{1/2} = -(1 + Nr \theta_w^3) \theta'(0). \quad (18)$$

The local Sherwood number is defined by

$$Sh_x = \frac{x q_m}{D_m (C_w - C_\infty)}, \quad (19)$$

where  $q_m$  is the mass transfer which is defined by

$$q_m = -D_m \left( \frac{\partial C}{\partial y} \right)_{y=0}, \quad (20)$$

Using the non-dimensional variables (7), we get from (19) and (20) as

$$Sh_x / Re_x^{1/2} = -\phi'(0). \quad (21)$$

where  $Re_x = \frac{u_w x}{\nu}$  is the local Reynolds number.

### 3. METHOD OF SOLUTION

Equations (8) – (12) together with the boundary conditions are solved numerically using the Runge-Kutta fifth order method along with shooting technique. To ensure the accuracy of the numerical method, results of the present analysis are compared with those of Hayat *et al.* [14], Mabood and Das [15], Mabood *et al.* [16] in the absence of  $E_1 = F^* = k_p = 0$ , and  $\varepsilon = 1.0$  in case of Newtonian fluid for different values of M. Table 1 shows that the results are in good agreement.

**Table-1:** Comparison of  $-f''(0)$  for various values of M when  $E_1 = F^* = k_p = 0$ ,  $\beta \rightarrow \infty$  and  $\varepsilon = 1.0$

M	Hayat et al. [14]	Mabood and Das [15]	Mabood et al. [16]	Present results
0	-1.00000	-1.000008	-1.0000084	-1.00000
1	1.4142	1.4142135	1.41421356	1.41421
5	2.4494	2.4494897	2.44948974	2.44949
10	3.31662	3.31662	3.316624	3.31662
50	7.14142	7.1414284	7.14142843	7.14142
100	10.04987	10.049875	10.0498756	10.04987
500	22.38302	22.383029	22.3830293	22.38302
1000	31.63858	31.638584	31.6385840	31.63858

### 4. RESULTS AND DISCUSSION

In this analysis numerical solutions are obtained to investigate the effect of various governing parameters on non-Darcy flow over a stretching surface in the presence of a magnetic field, electrical field, non-linear thermal radiation, viscous dissipation and chemical reaction. The computational results are shown through graphs and discussed.

Fig. 2 reveals that the velocity decreases throughout the boundary layer region which leads to thinning of the boundary layers for increasing values of Casson parameter( $\beta$ ). The temperature and concentration increase with increasing values of  $\beta$  as illustrated in Figs. 3 and 4. The corresponding thermal and solutal boundary layers become thicker. Fig. 5 shows that the effect of magnetic parameter is to diminish the velocity distribution in the boundary layer leading to thinning of the boundary layer. This is due to the Lorentz force developed due to the transverse magnetic field, which resists the fluid motion. As a result temperature and concentration of the fluid are seen to increase with increase in M (Figs. 6 and 7) and the thickness of the associated thermal and solutal boundary layers is increased.

The variation of porosity parameter ( $\varepsilon$ ) of porous medium is plotted in Figs. 8 – 10. For an increase in the value of the porosity parameter, velocity distribution in the fluid flow increases whereas temperature and concentration are seen to decrease. Figs. 11 – 13 depict the influence of inertial parameter ( $F^*$ ) on the velocity, temperature and concentration. It is clear from Fig. 14 that the velocity gets diminished with increase in the value of  $F^*$  while a reversal trend in temperature and concentration is found. Fig. 14 illustrates that electric parameter ( $E_1$ ) increases the velocity distribution throughout the hydrodynamic boundary layer in the vicinity of the boundary. However, a little away from the stretching sheet, the enhancement in velocity is more pronounced. Fig. 15 shows that temperature is dropped for an increase in electric field parameter due to increase in the mass flux. Species concentration shows a reduction for an increase in  $E_1$  (Fig. 16). Fig. 17 indicates that velocity distribution shows a decreasing tendency with increasing values of porous permeability parameter( $k_p$ ), as expected and consequently the temperature and concentration distributions are increased (Figs. 18 and 19).

Fig. 20 depicts that the temperature is a decreasing function of Prandtl number (Pr) in the thermal boundary layer. For higher Prandtl number fluids, the thermal diffusivity is smaller. Hence, increasing values of Prandtl number result in decrease in the temperature. Fig. 21 shows that larger values of Nr imply enhanced radiation which leads to increase in temperature. From Fig. 22 it is clear that the variation of temperature ratio parameter ( $\theta_w$ ) is similar to that of the radiation parameter. Fig. 23 depicts that increased values of Eckert number (Ec) enhance the temperature due to release of energy due to frictional heating and hence temperature raises. When Ec assumes values greater than 0.7, an over shoot above the prescribed value of the surface temperature occurs on the boundary.

Fig. 24 shows that Schmidt's number (Sc) decreases the concentration as expected and hence the thickness of the solutal boundary layer reduces for higher values of Sc. The effect of chemical reaction ( $\gamma$ ) on concentration distribution is plotted in Fig. 25. The concentration from its assigned peak value that is unity on the boundary begins to diminish till it attains its minimum value of zero at far upstream. As the chemical reaction parameter takes larger values, it is found that the concentration decreases further. Fig. 26 shows that the surface drag coefficient decreases with increasing values of Casson parameter as well as magnetic field parameter. From Fig. 27 it is observed that with increasing values of the radiation parameter the Nusselt number decreases while it enhances with Prandtl number. It is clear from Fig. 28 that increased values of Schmidt number and chemical reaction parameter enhance the local Sherwood number.

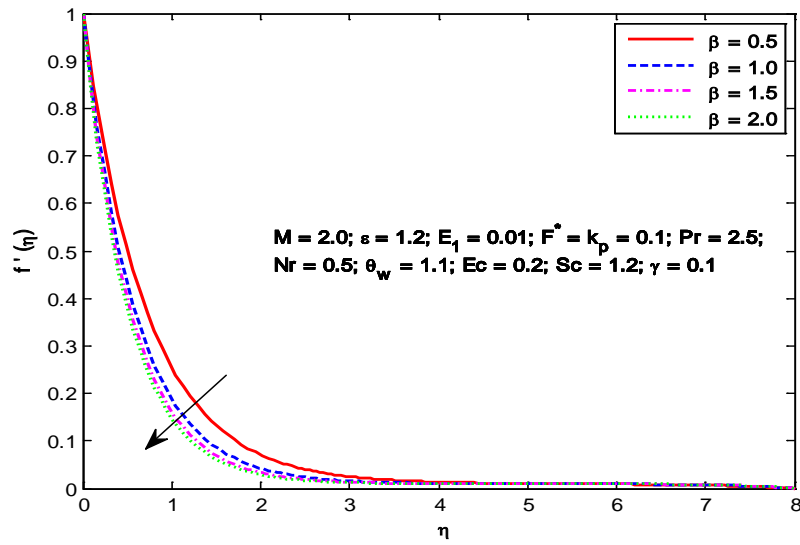


Figure-2: Velocity profiles for different Values of  $\beta$

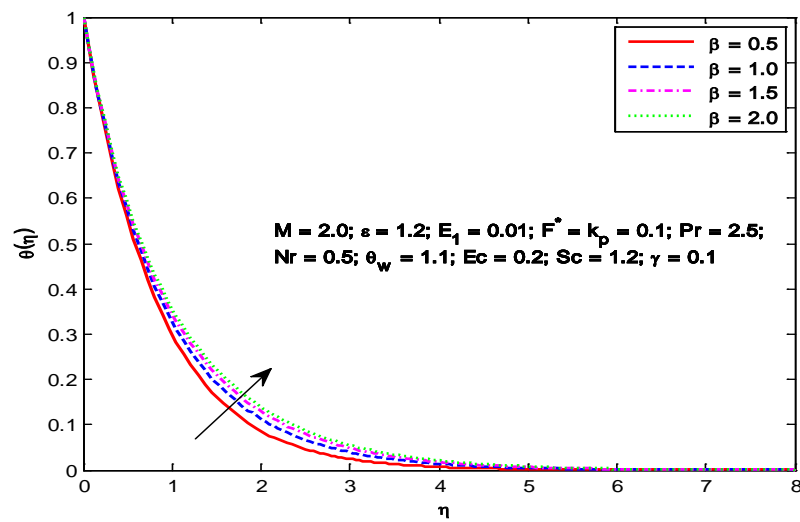


Figure-3: Temperature profiles for different values of  $\beta$

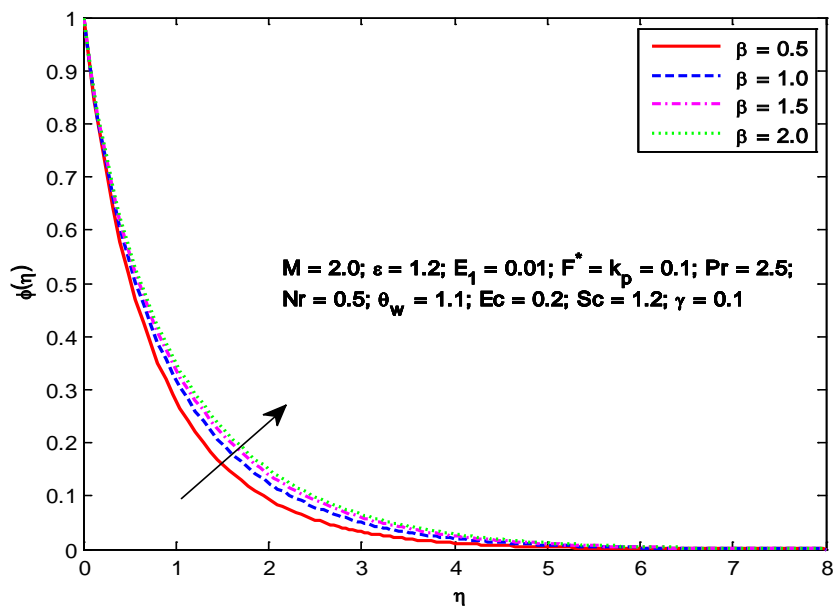


Figure-4: Concentration profiles for different values of  $\beta$

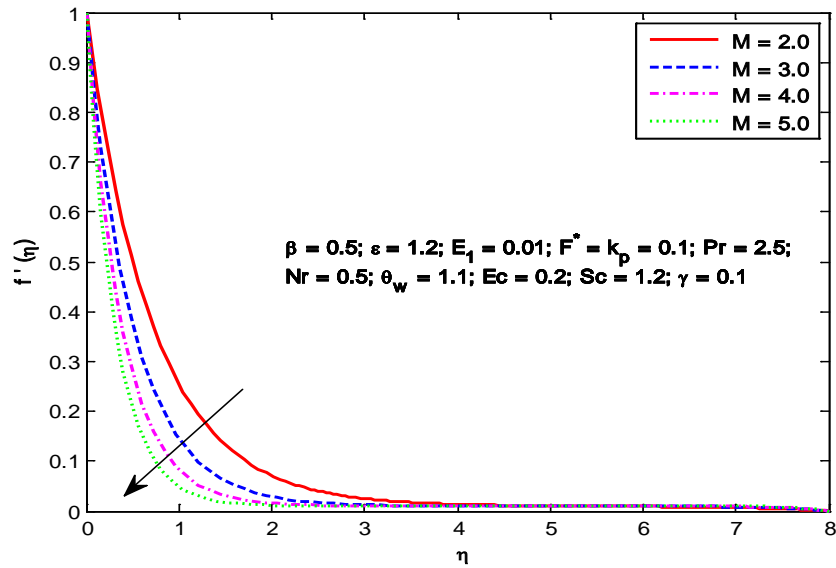


Figure-5: Velocity profiles for different Values of M

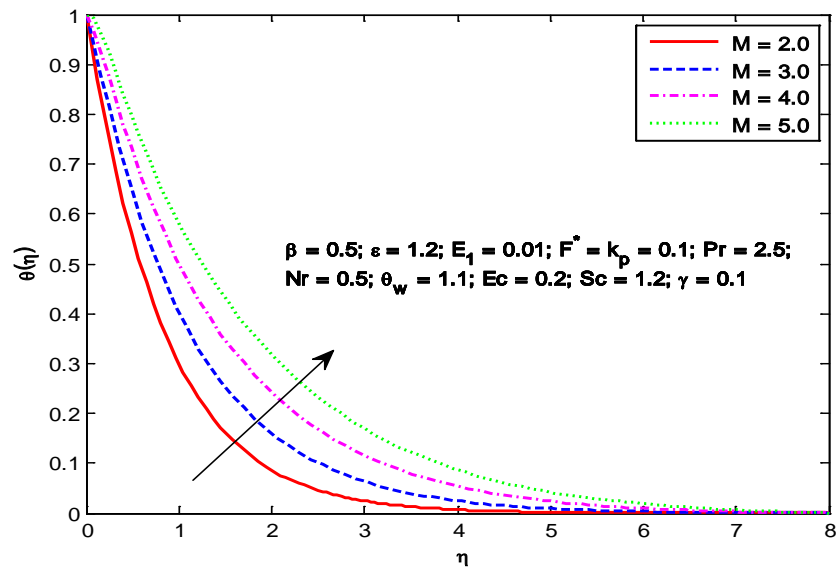


Figure-6: Temperature profiles for different values of M

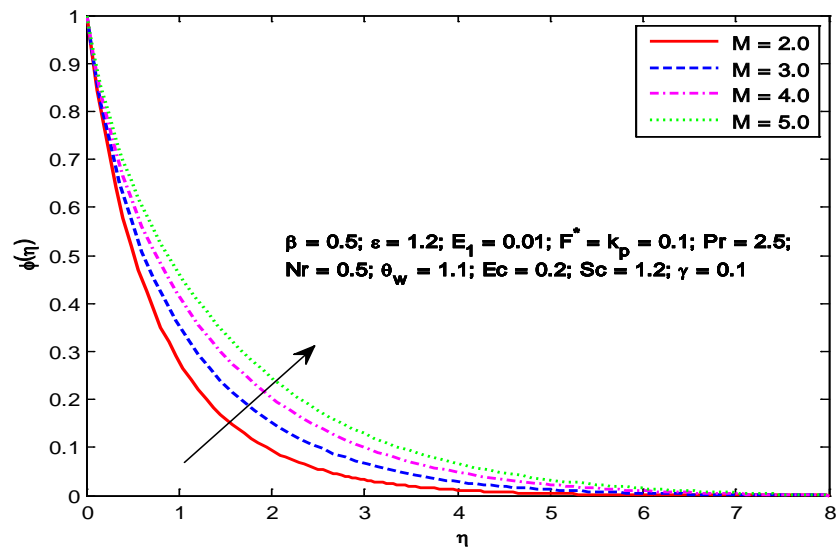


Figure-7: Concentration profiles for different values of M

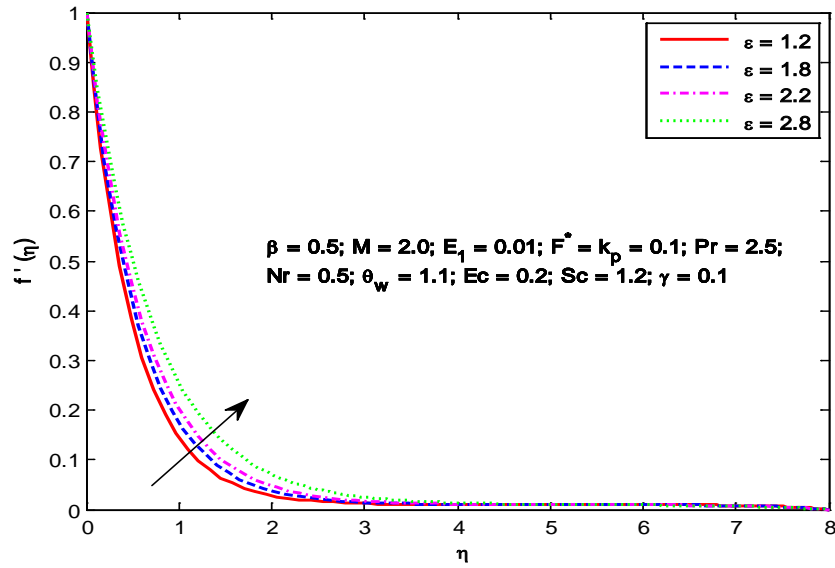


Figure-8: Velocity profiles for different Values of  $\varepsilon$

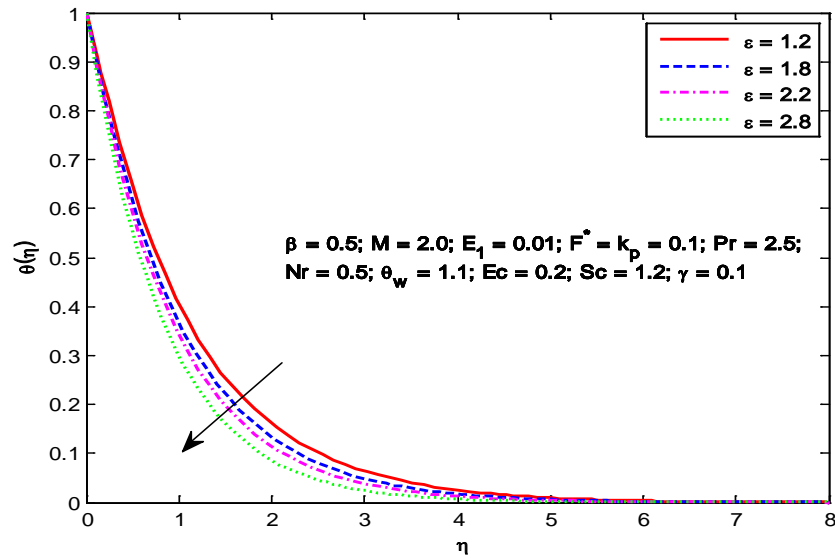


Figure-9: Temperature profiles for different values of  $\varepsilon$

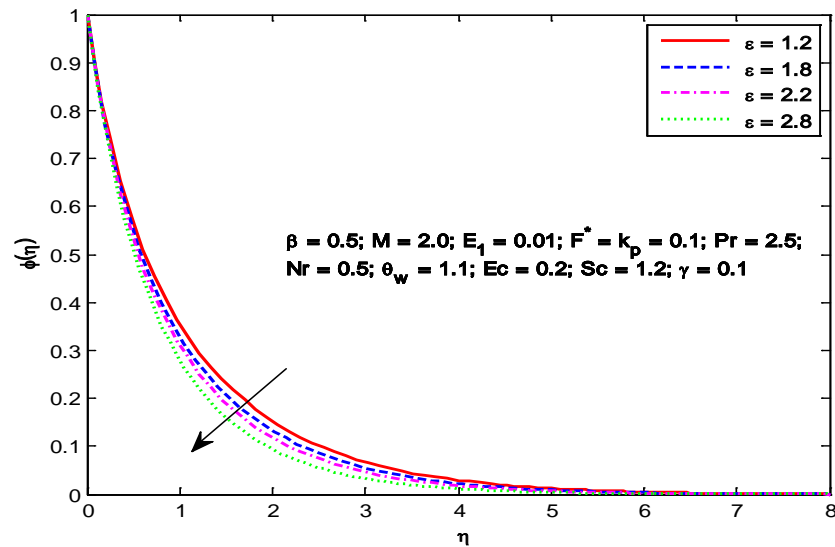


Figure-10: Concentration profiles for different values of  $\varepsilon$

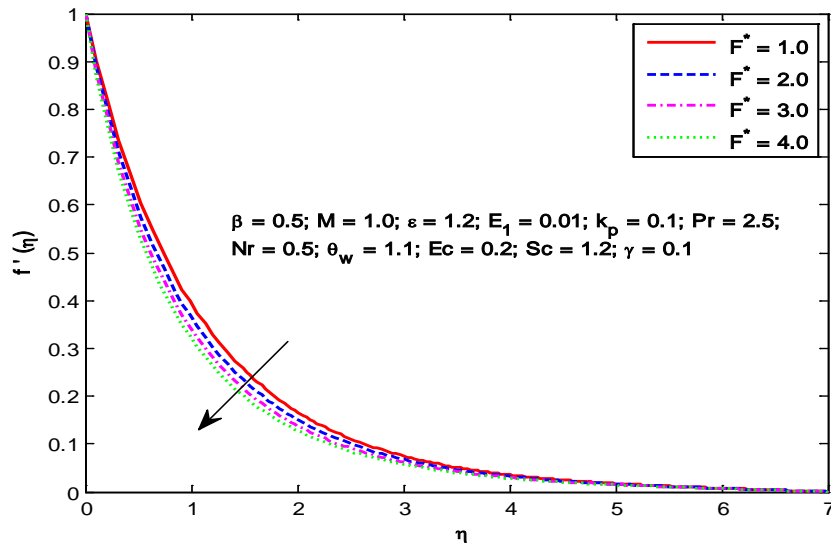


Figure-11: Velocity profiles for different Values of  $F^*$

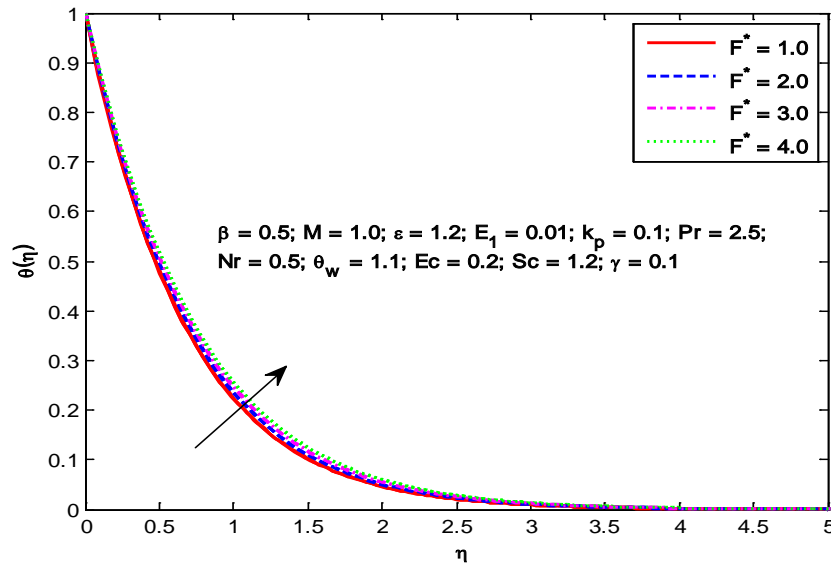


Figure-12: Temperature profiles for different values of  $F^*$

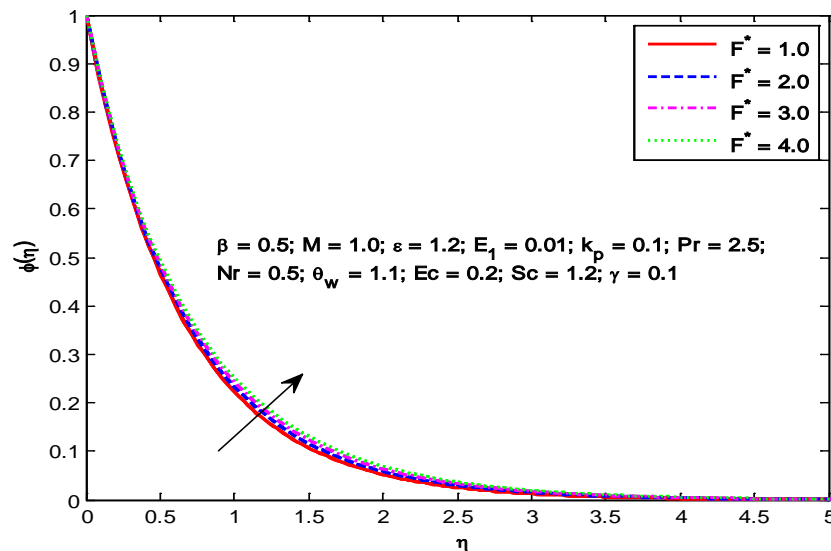


Figure-13: Concentration profiles for different values of  $F^*$



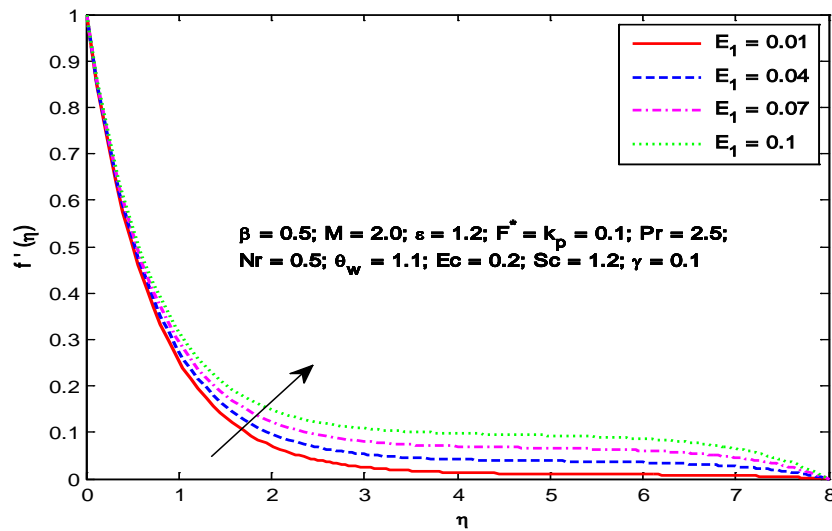


Figure-14: Velocity profiles for different Values of  $E_1$

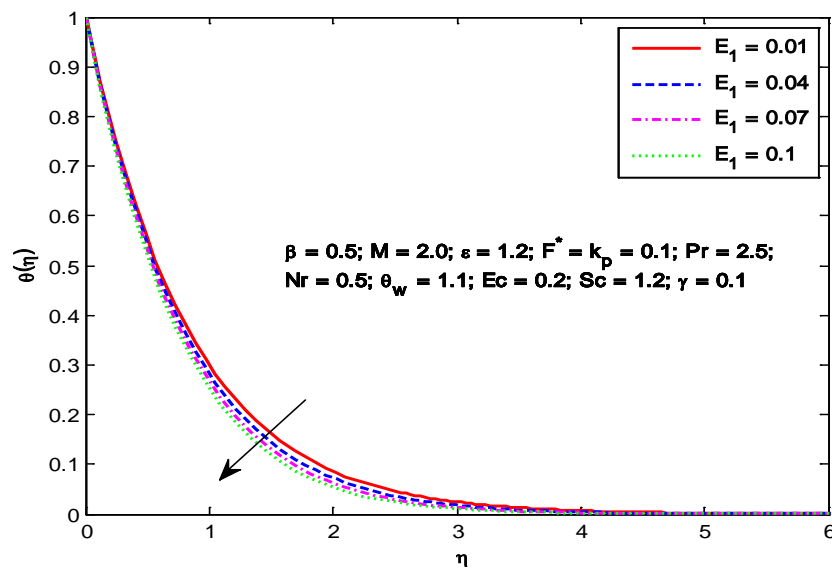


Figure-15: Temperature profiles for different values of  $E_1$

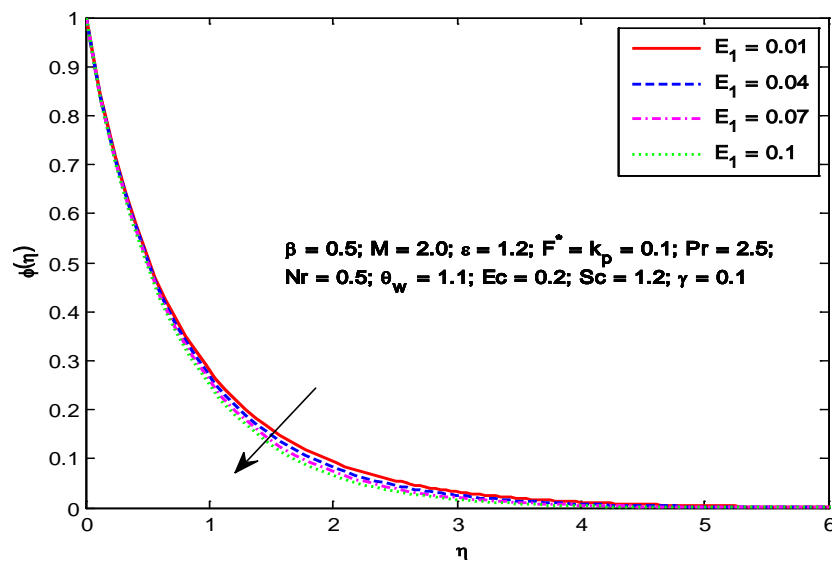


Figure-16: Concentration profiles for different values of  $E_1$

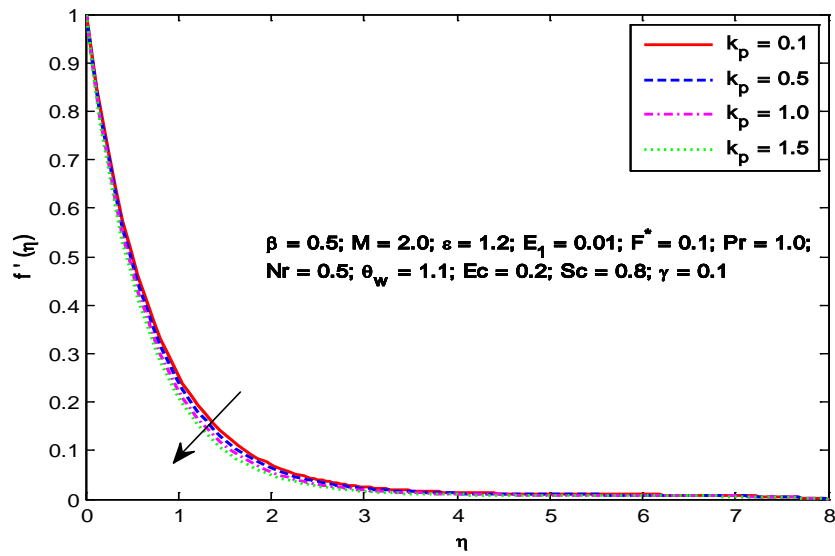


Figure-17: Velocity profiles for different Values of  $k_p$

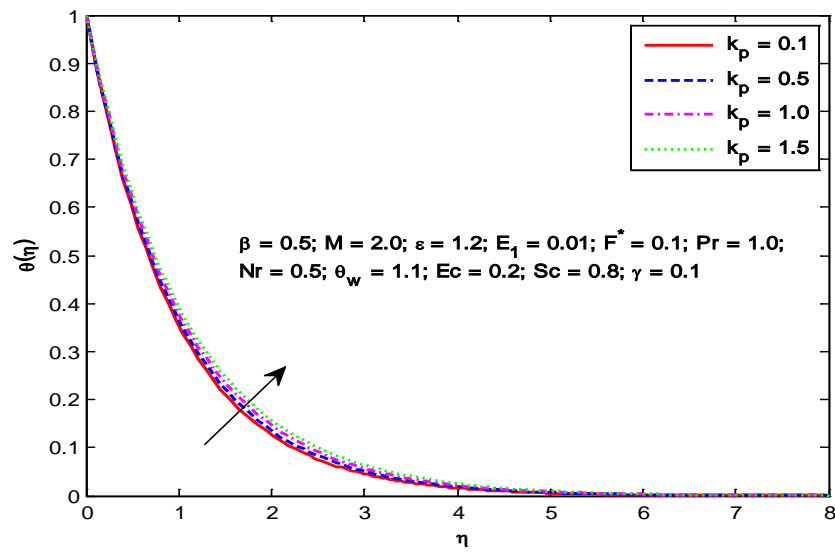


Figure-18: Temperature profiles for different values of  $k_p$

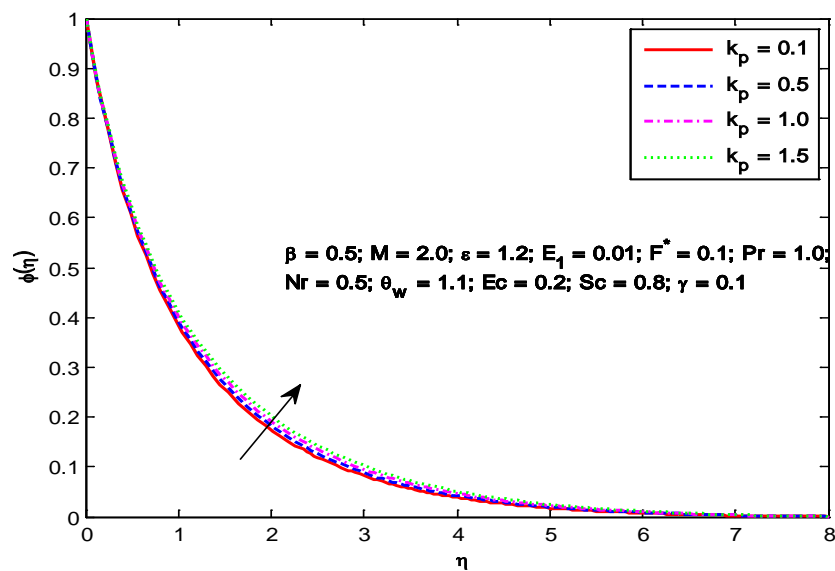
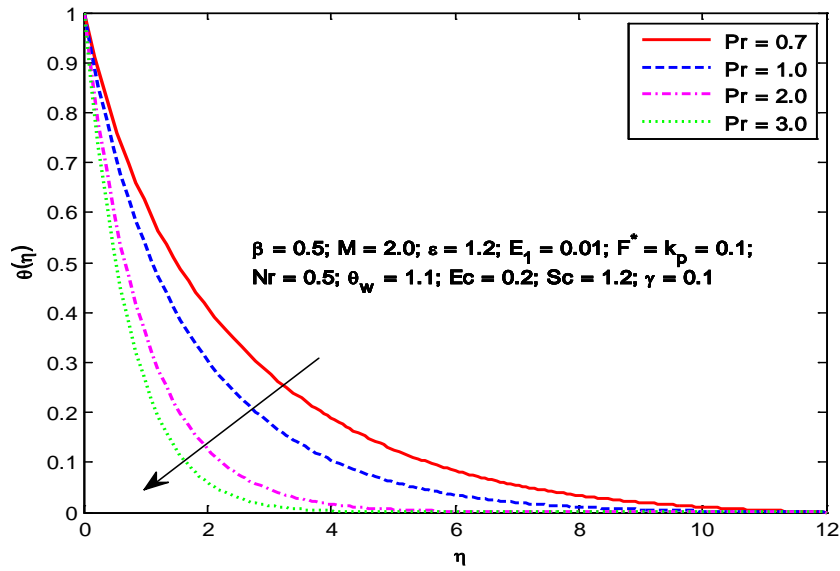
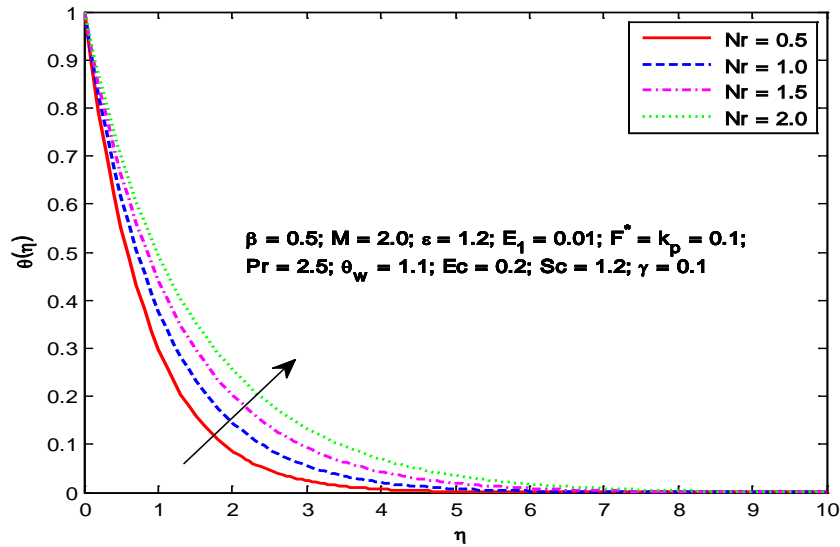


Figure-19: Concentration profiles for different values of  $k_p$



**Figure-20:** Temperature profiles for different values of Pr



**Figure-21:** Temperature profiles for different values of Nr

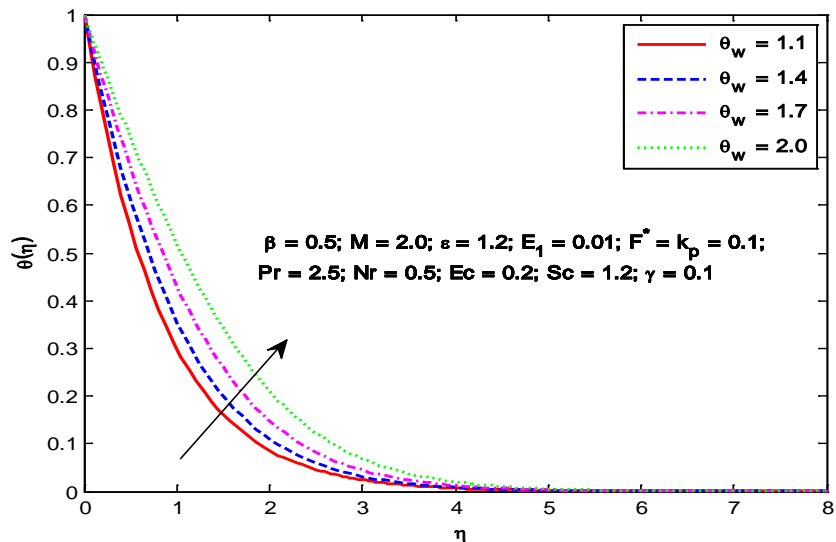


**Figure-22:** Temperature profiles for different values of  $\theta_w$

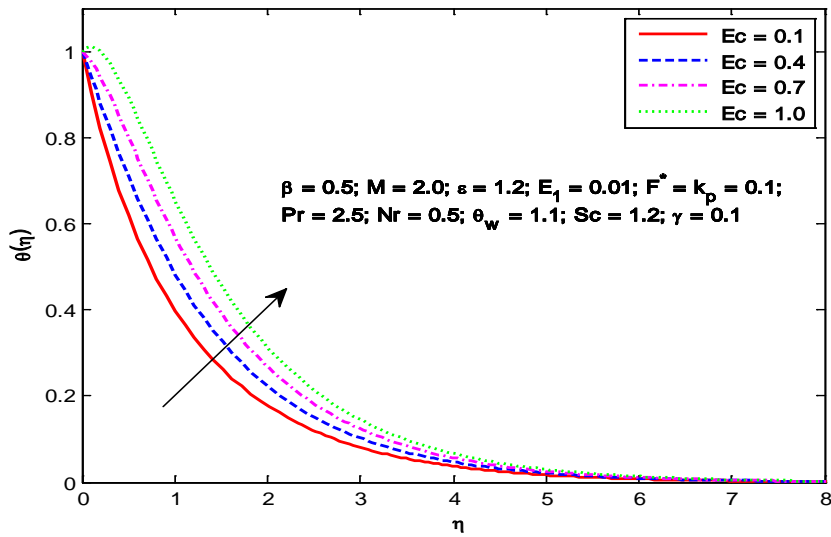


Figure-23: Temperature profiles for different values of Ec

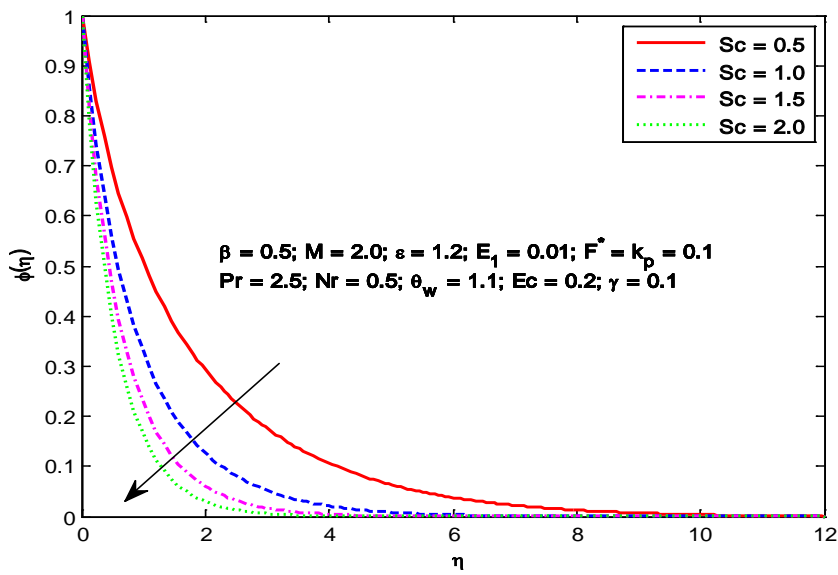


Figure-24: Concentration profiles for different values of Sc

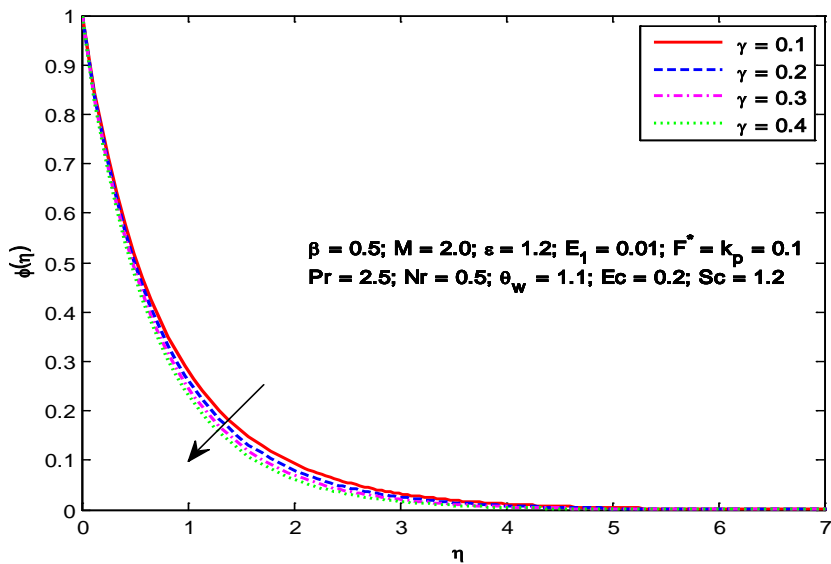


Figure-25: Concentration profiles for different values of  $\gamma$

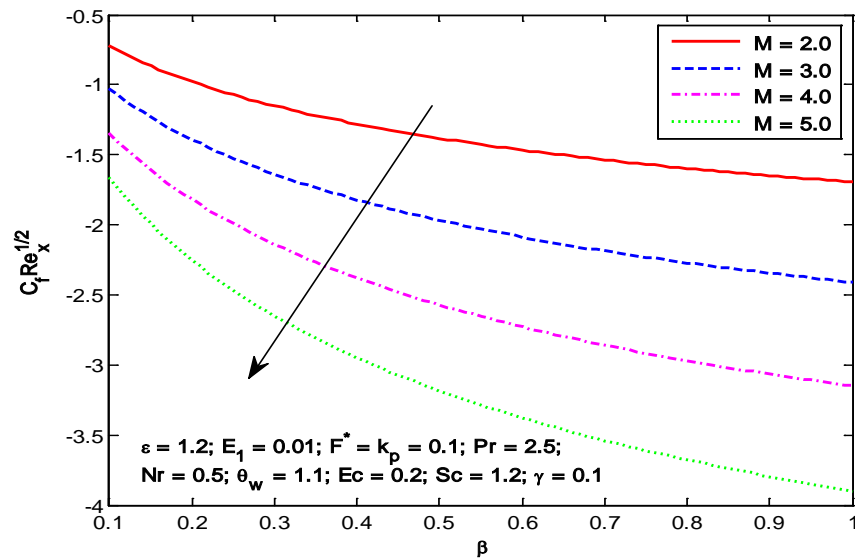


Figure-26: Variation of skin friction coefficient with  $\beta$  for different values of  $M$

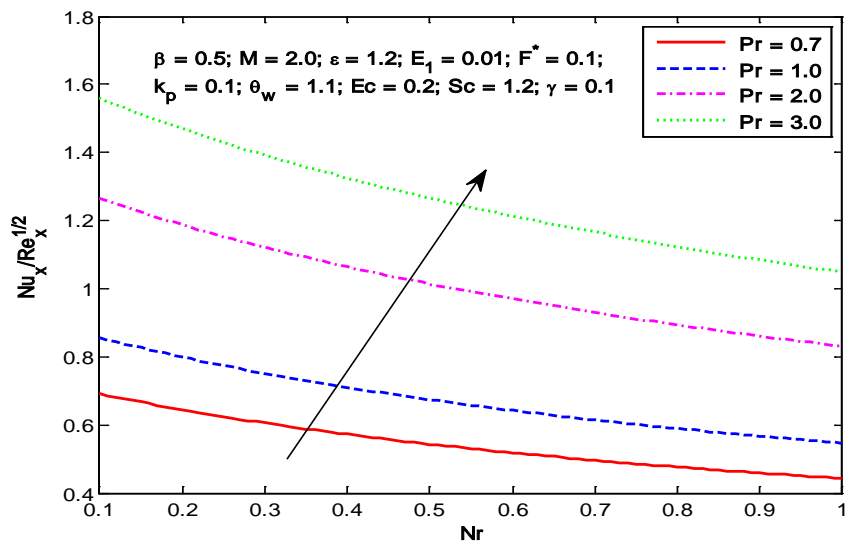


Figure-27: Variation of Nusselt number with  $Nr$  for different values of  $Pr$

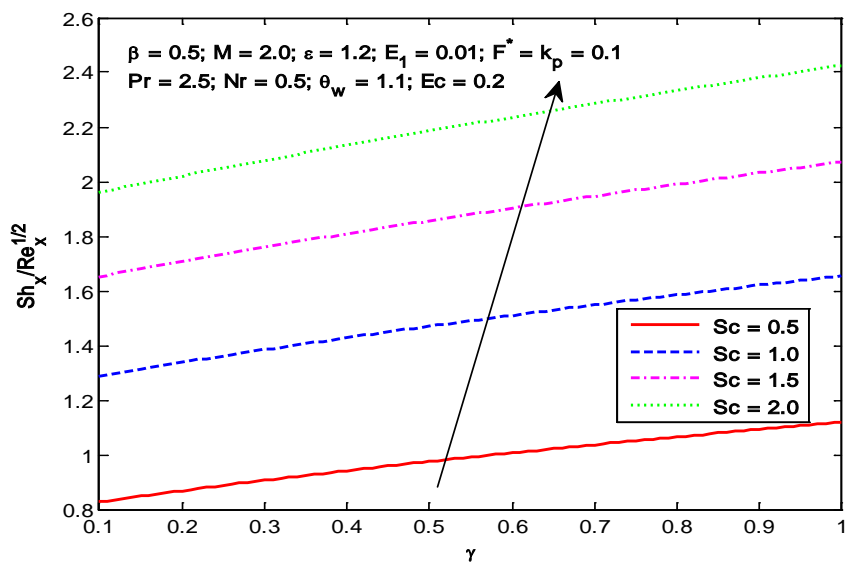


Figure-28: Variation of Sherwood number with  $\gamma$  for different values of  $Sc$

## 5. CONCLUSIONS

The salient findings of this investigation are summarized as follows:

- For larger values of Casson parameter, the velocity decreases.
- Stronger Lorentz force retards the fluid flow and increases the temperature.
- Electrical force accelerated the flow giving rise to higher velocities
- Inertial parameter decreased the velocity while temperature and concentration of the fluid are enhanced.
- Increasing temperature ratio parameter raises the temperature distribution of the fluid.
- Schmidt number and chemical reaction parameter produced thinner solutal boundary layers with a reduction in concentration.
- The rate of heat transfer is enhanced by radiation parameter.

## REFERENCES

1. Tammamasi B., Considucution of certain haemorhological Phenomenon from the Haemorheology, 89 (1968), Pergamom press, London.
2. Walwander W. P., Chen T. Y., Cala. D. F., An approximate Casson fluid model for tube flow of blood, Biorheology, 12 (1975), 111–119.
3. Vinogradov G. V., Malkin A. Y., Rheology of polymers, Mir Publisher, Moscow, (1979).
4. Mustafa M., Hayat T., Pop I., Aziz A., Unsteady boundary layer flow of a Casson fluid due to an impulsively started flat plate, Heat Transfer – Asian Research, 40 (2011), 563–576.
5. Pramanik S., Casson fluid flow and heat transfer past an exponentially porous stretching surface in presence of thermal radiation, Ain Shams Engineering Journal, 5 (2013), 205–212.
6. Shehzad S. A., Hayat T., Qasim M., Asghar S., Effects of mass transfer on MHD flow of Casson fluid with chemical reaction and suction, Brazilian Journal of Chemical Engineering, 30 (2013), 187–195.
7. Nadeem S., Rashid Mehmood, Noren Sher Akbar, Optimezed analytical solution for oblique flow of a Casson-nano fluid with convective boundary conditions” Internal Journal of Thermal Science, 78 (2014), 90–100.
8. Mahanta G., Shaw S., 3D Casson fluid flow past a porous linearly stretching sheet with convective boundary condition, Alexandria Engineering Journal, 54 (2015), 653–659.
9. Sarojamma G., Sreelakshmi K., Vasundhara B., Mathematical Model of MHD Unsteady Flow Induced by a Stretching Surface Embedded in a Rotating Casson Fluid with Thermal Radiation, 978-9-3805-4421-2/16/\$31.00\_c 2016 IEEE, (2016), 1590–1595.
10. Nield N. A., Bejan A., Convection in porous media, Fourth ed. Springer-Verlag, New York, (2013).
11. Cortell R., Fluid flow and radiative nonlinear heat transfer over stretching sheet, Journal of King Saud University – Science, 26 (2013), 161–167.
12. Mushtaq A., Mustafa M., Hayat T., Alsaedi A., Nonlinear radiative heat transfer in the flow of nanofluid Due To solar energy: A numerical study, Journal of the Taiwan Institute of Chemical Engineers, 45 (2014), 1176–1183.
13. Hayat T., Imtiaz M., Alsaedi A., Kutbi, M. A., MHD three dimensional flow of nanofluid with velocity slip and nonlinear thermal radiation, Journal of Magnetism and Magnetic Materials, 396 (2015), 31–37.
14. Hayat T., Hussain Q., Javed T., The modified decomposition method and pade approximations for the MHD flow over a non-linear stretching sheet, Nonlinear Anal. Real World Appl., 10 (2009), 966–973.
15. Maboob F., Das K., Melting heat transfer on hydromagnetic flow of a nanofluid over a stretching sheet with radiation and second order slip, European Phys. J. Plus, 131 (2016), 1–12.
16. Maboob F., Imtiaz M., Alsaedi A., Hayat T., Unsteady convective boundary layer flow of Maxwell fluid with nonlinear thermal radiation: A numerical study, Int. J. Nonlinear Sciences and Numerical Simulation, (2016), 1–9.

**Source of support: Nil, Conflict of interest: None Declared.**

**[Copy right © 2016. This is an Open Access article distributed under the terms of the International Journal of Mathematical Archive (IJMA), which permits unrestricted use, distribution, and reproduction in any medium, provided the original work is properly cited.]**